Temperature- and pressure-driven spin-state transitions in $LaCoO_3$

D. P. Kozlenko,[1] N. O. Golosova,[1] Z. Jirák,[2] L. S. Dubrovinsky,[3] B. N. Savenko,[1] M. G. Tucker,[4] Y. Le Godec,[5] and V. P. Glazkov[6]

[1]*Frank Laboratory of Neutron Physics, JINR, 141980 Dubna, Russia*

[2]*Institute of Physics, Cukrovarnická 10, 162 53 Prague 6, Czech Republic*

[3]*Bayerisches Geoinstitut, Universität Bayreuth, Bayreuth, D-95440, Germany*

[4]*ISIS Facility, Rutherford Appleton Laboratory, Chilton, Oxon, OX11 0QX, United Kingdom*

[5]*Physique des Milieux Condensés, Université P&M Curie, B77, 4 Place Jussieu, 75252 Paris, France*

[6]*Russian Research Center "Kurchatov Institute," 123182 Moscow, Russia*

(Received 23 January 2006; revised manuscript received 26 December 2006; published 26 February 2007)

Crystal structure, spin state, and semiconductor-metal transitions of $LaCoO_3$ in the 10–905 K temperature range were studied by neutron diffraction at high pressures up to 4.5 GPa and x-ray diffraction and Raman spectroscopy at high pressures up to 17.5 GPa. The susceptibility and thermal-expansion anomalies in the studied pressure range can be described successfully by the thermal excitation of two orbitally nondegenerate magnetic states with different electronic configuration, intermediate spin (IS), and high spin (HS) from the low-spin (LS) nonmagnetic ground state. The pressure-induced compression of Co-O bonds leads to a substantial increase of LS-IS and LS-HS energy splittings E_1 and E_2 with $d\ln E_1/dP=0.37$ and $d\ln E_2/dP=0.23$ GPa^{-1}. The onset of the semiconductor-metal (S-M) transition in $LaCoO_3$ correlates with the vanishing of several Raman modes forbidden for rhombohedral $R\bar{3}c$ symmetry and originating from local distortions due to short-range e_g-orbital order of IS Co^{3+} ions. The S-M transition temperature increases rapidly under pressure with $dT_{S\text{-}M}/dP \approx 50$ K/GPa.

DOI: 10.1103/PhysRevB.75.064422 PACS number(s): 61.12.−q, 61.10.Nz, 78.30.Hv, 71.30.+h

I. INTRODUCTION

Among the rare-earth transition-metal oxides with perovskitelike structure the lanthanum cobaltite $LaCoO_3$ exhibits unusual electronic and magnetic properties at ambient pressure.[1–4] At low temperature $LaCoO_3$ is a nonmagnetic semiconductor with a ground state of Co^{3+} ions of a low-spin (LS) configuration (t_{2g}^6, $S=0$). As temperature increases, a sharp anomaly in the magnetic susceptibility corresponding to the appearance of the paramagnetic state was observed at $T\sim 100$ K and a gradual semiconductor-metal (S-M) transition accompanied by another broad anomaly in the magnetic susceptibility occurs at $T\sim 500$ K. Both susceptibility anomalies are also associated with the anomalies in the thermal lattice expansion.[1–4] Despite numerous studies of structural, magnetic, and electronic properties, the nature of the thermally driven spin-state transitions from the initial nonmagnetic to the paramagnetic states with different effective paramagnetic moment values at $T\sim 100$ and 500 K is still extensively debated. Originally Goodenough[3,5] proposed that the crystal-field splitting energy of the ground state of the Co^{3+} ions is comparable with the intra-atomic exchange energy. It was assumed that the energy gap between the t_{2g} and e_g states is rather small, ~10 meV, therefore t_{2g} electrons can be thermally exited from the LS into the high-spin (HS) ($t_{2g}^4e_g^2$, $S=2$) state. Above 100 K, a possibility of the LS-HS ordered superstructure was also suggested,[3–5] but not experimentally confirmed.[6,7]

However, the simple LS-HS model was incompatible with the temperature behavior of photoemission[8] and the x-ray-absorption[9,10] spectra demonstrated very subtle changes in the region of the nonmagnetic-paramagnetic transition at $T\sim 100$ K and sharp changes were observed at $T\sim 500$ K only, corresponding to the second susceptibility anomaly and the S-M transition. Subsequently, an existence of the intermediate spin (IS) state ($t_{2g}^5e_g^1$, $S=1$) was proposed[11] and supported by LDA+U calculations,[12] which have shown that the HS state is actually located at higher energy and the paramagnetic transition at $T\sim 100$ K comes due to the population of the IS state stabilized by the hybridization of Co e_g and O $2p$ orbitals.

The three-level LS-IS-HS model was found to provide a qualitative description of the two anomalies of the magnetic susceptibility and thermal expansion in the extended temperature range.[13,7] For the intermediate temperatures below the second anomaly, the simpler LS-IS scenario becomes the most widely accepted and it was supported by recent high-resolution x-ray absorption and photoemission,[14,15] susceptibility and thermal expansion,[16–18] heat capacity,[19] and inelastic neutron-scattering[20] investigations.

ESR measurements provided evidence that at low temperatures $T<50$ K the first excited state of Co^{3+} is the triplet with the zero-field splitting of 0.6 meV.[21] It was attributed to the HS state, which splits by spin-orbit coupling into the lowest-lying triplet (with effective total angular momentum $\tilde{J}=1$) and higher-lying quintet and septet.[21,22] However, obtained from the ESR value of a g factor about 3.5 is inconsistent with magnetic susceptibility, giving about three times larger susceptibility values.[21] It is also in conflict with the absence of pronounced changes in x-ray absorption and photoemission spectra at low temperature, expected for the HS-state appearance.[8–10,14] Alternatively, it was shown that the susceptibility and thermal expansion in the intermediate temperature range can be described well in terms of the orbitally nondegenerate IS-state excitation with a g-factor value ~2.[16–18]

The presence of the Co^{3+} ions in the IS state with partially occupied e_g orbitals, which have a strong Jahn-Teller (JT) nature, imply the possibility of the orbital order in $LaCoO_3$.[12] Neutron-diffraction investigations[6,7] have shown that the crystal structure of $LaCoO_3$ is rhombohedral (sp. gr. $R\bar{3}c$), which does not allow the static cooperative JT distortion of CoO_6 octahedra. Afterwards the monoclinic distortion ($I2/a$ symmetry) of the crystal structure of $LaCoO_3$ was found from high-resolution x-ray diffraction and it was attributed to a static cooperative JT distortion, associated with the long-range e_g orbital order.[23] The local static JT distortion was also suggested from a pair density function analysis of neutron-scattering data.[24] In addition, a number of infrared[25,26] and Raman[27,28] active modes forbidden for the $R\bar{3}c$ symmetry was observed in $LaCoO_3$ at $T<300$ K and their relevance to the orbital order was suggested.[26–28] However, more recent inelastic neutron-scattering experiments[20] have demonstrated that the orbital order is of short-range dynamic character with a correlation length of about 3.6 Å, comparable to Co-O distance. A decrease of the intensity of Raman modes forbidden for the $R\bar{3}c$ symmetry under laser surface heating and their disappearance at surface temperature estimated to be close to the semiconductor-metal transition temperature was established,[29] signaling the possible "melting" of the orbital order in the metallic state.

Recent magnetic susceptibility,[30] x-ray diffraction,[31] and photoemission spectroscopy[14] investigations have shown that the balance between different spin states in $LaCoO_3$ can be strongly changed by the application of high pressure in the favor of the LS state. However, a relationship between pressure-induced variation of structural parameters, namely, Co-O and Co-O-Co bond lengths and angles, and energy splittings mediating the population of the nonmagnetic ground and magnetic excited states in $LaCoO_3$ remains unclear, as well as a behavior of S-M transition temperature and orbital ordering under pressure. This information is crucial for understanding the nature of spin-state transitions and related phenomena in $RCoO_3$ cobaltites in general.

In order to study high-pressure effects on the crystal structure, spin state, and semiconductor-metal transitions of $LaCoO_3$, we have performed the combined neutron, x-ray diffraction, and Raman spectroscopy investigations over 0–17.5 GPa pressure and 10–905 K temperature ranges.

II. EXPERIMENTAL DETAILS

The synthesis procedure of the $LaCoO_3$ sample and the details of susceptibility measurements are described in Ref. 18. Neutron powder diffraction measurements at high pressures up to 4.5 GPa in the low-temperature range 10–250 K were performed with the DN-12 diffractometer[32] at the IBR-2 pulsed reactor (FLNP JINR, Dubna, Russia) using the sapphire anvil pressure cells.[33] The pressure was determined by the ruby fluorescence technique. Diffraction patterns were collected at the scattering angle $2\theta=90°$ with the resolution $\Delta d/d\approx 0.015$.

Due to technical restrictions the sapphire anvil high-pressure technique could not be used at sufficiently high temperatures, and neutron powder diffraction measurements at ambient and high-pressure $P=3.7$ GPa in the temperature range 300–905 K were performed using the Pearl/HiPr diffractometer at the ISIS pulsed neutron spallation source (RAL, UK). In order to determine pressure dependences of structural parameters at ambient temperature, several points in the pressure range 0–3.7 GPa were also measured. The high P-T setup[34] for the Paris-Edinburgh high-pressure cell was used. The sample in the MgO capsule (used as a pressure marker[35]) was placed into a graphite furnace that was loaded into the pyrophyllite gasket. The heat was generated by electrical current and the temperature value on the sample was measured by the neutron absorption resonance radiography technique[36] using tantalum and hafnium foils also placed into the MgO capsule. Diffraction patterns were collected by a detector bank covering the scattering angle range $83° < 2\theta < 97°$ with the resolution $\Delta d/d\approx 0.008$. The diffraction data were analyzed by the Rietveld method using either MRIA[37] (DN-12) or the General Structure Analysis System (GSAS)[38] (Pearl/HiPr).

X-ray powder diffraction and Raman spectroscopy measurements were made at high pressures up to 17.5 GPa with a diamond anvil cell.[39] The sample was loaded in the Re gasket with a 4:1 methanol-ethanol mixture as a pressure transmitting medium. The pressure was measured using the ruby fluorescence technique. The x-ray-diffraction spectra were measured at the system consisting of a high-brilliance FRD rotating anode generator (Mo K_α radiation, $\lambda=0.7115$ Å), FluxMax focusing optics, and Bruker APEX CCD area detector. The two-dimensional XRD images were converted to conventional one-dimensional diffraction patterns using the FIT2D program.[40] The data analysis was performed using the FULLPROF program.[41] Raman spectra were collected using LabRam spectrometer (NeHe excitation laser with wavelength 632 nm, grating 1800, confocal hole 11 μm, $\times 50$ objective).

III. RESULTS

A. Crystal structure and spin-state transitions

The pressure dependences of the unit-cell volume and lattice parameters for $LaCoO_3$, derived from the x-ray-diffraction measurements at ambient temperature, are shown in Fig. 1. The volume compressibility data were fitted by the Birch-Murnaghan equation of state:[42]

$$P=\frac{3}{2}B_0(x^{-7/3}-x^{-5/3})\left[1+\frac{3}{4}(B'-4)(x^{-2/3}-1)\right], \quad (1)$$

where $x=V/V_0$ is the relative volume change, V_0 is the unit-cell volume at $P=0$, and B_0, B' are the bulk modulus $[B_0=-V(dP/dV)_T]$ and its pressure derivative $[B'=(dB_0/dP)_T]$. The calculated values $B_0=165(5)$ GPa and $B'=4$ as well as linear compressibilities $k_i=-(1/a_{i0})(da_i/dP)_T$ $(a_i=a,c)$ of lattice parameters $k_a=0.0015(3)$ and $k_c=0.0019(2)$ GPa^{-1}, are comparable with those obtained previously for $LaCoO_3$ and $La_{0.82}Sr_{0.18}CoO_3$ in the smaller pressure range.[31,43]

The neutron diffraction patterns of $LaCoO_3$ measured at selected pressures and temperatures with the Pearl/HiPr and

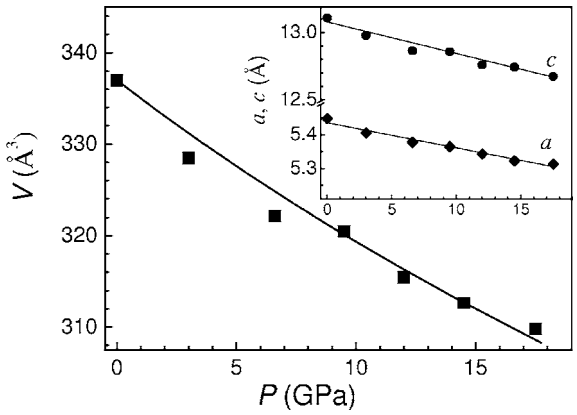

FIG. 1. Pressure dependences of the unit-cell volume fitted by the Birch-Murnaghan equation of state and lattice parameters (in the hexagonal setting, inset) of $LaCoO_3$ at ambient temperature fitted by linear functions.

DN-12 diffractometers are shown in Figs. 2 and 3. The data were treated using the conventional rhombohedral ($R\bar{3}c$) model of the crystal structure and the structural parameters obtained at ambient pressure were similar to ones found in previous studies.[6,7] As the pressure increases the Co-O bond length decreases nearly linearly and the Co-O-Co bond angle

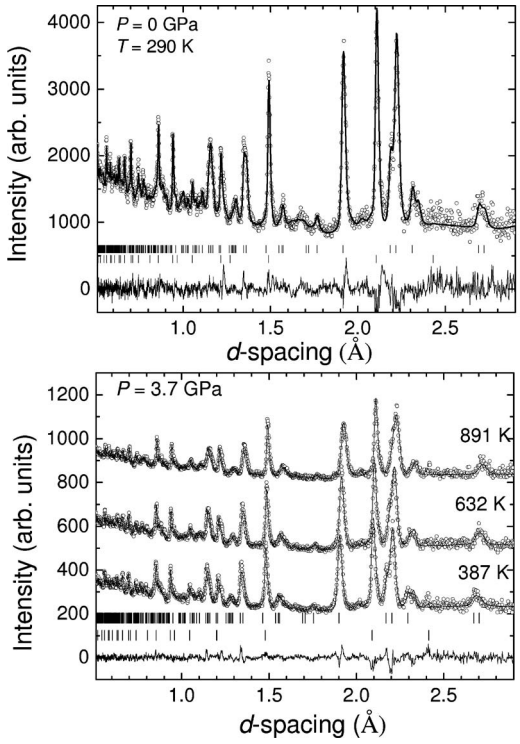

FIG. 2. Neutron diffraction patterns of $LaCoO_3$ measured at ambient conditions (top) and $P=3.7$ GPa, $T=387$, 632, and 891 K (bottom) at the Pearl/HiPr diffractometer and processed by the Rietveld method. The experimental points, calculated profiles, and difference curves (for ambient conditions and $P=3.7$ GPa, $T=387$ K) are shown. The ticks below represent positions of diffractions peaks of $LaCoO_3$ (upper row) and MgO sample container which was used in high-pressure measurements (lower row).

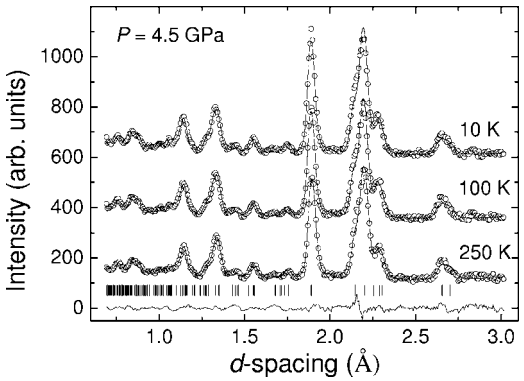

FIG. 3. Neutron diffraction patterns of $LaCoO_3$ measured at $P=4.5$ GPa, $T=10$, 100, and 250 K at the DN-12 diffractometer and processed by the Rietveld method. The experimental points, calculated profiles and difference curve for $T=250$ K are shown. The ticks below represent positions of diffraction peaks of $LaCoO_3$.

increases slightly at ambient temperature (Fig. 4). The linear compressibility of the Co-O bond length $k_{\text{Co-O}}=0.0024(3)$ GPa^{-1} is comparable with that for compounds $La_{0.7}Sr_{0.3}CoO_3$ and $La_{0.7}Sr_{0.3}MnO_3$ having similar rhombohedral structure.[44,45]

The anomalous part of the thermal unit-cell volume expansion $Q=(V-V_T)/V_T$ obtained from neutron diffraction data at ambient pressure, where V_T described the normal thermal expansion due to phonons and calculated as in Ref. 7, is shown in Fig. 5. It looks similar to the data of Refs. 7 and 13. The magnetic susceptibility χ at ambient pressure corrected for the paramagnetic impurity contribution and diamagnetic contribution from the core electrons is also shown in Fig. 5.

The presence of two correlated anomalies in the thermal expansion and susceptibility in the 0–800 K range, as well as particular behavior of x-ray absorption and photoemission spectra[8–10,14,15] and the increase of the effective paramagnetic moment from $\mu_{eff}=3.4\mu_B$ ($150<T<350$ K) to $\mu_{eff}=4.1\mu_B$ ($T>650$ K) (Ref. 4) in $LaCoO_3$ can be explained quite naturally if two successive changes of the spin state of Co^{3+} occur. The LDA+U calculations[12] predict the relative difference between energies of two excited states in $LaCoO_3$

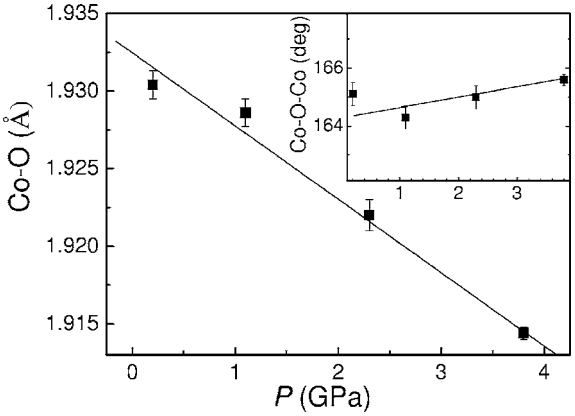

FIG. 4. Pressure dependences of the Co-O bond length and Co-O-Co angle (inset) at ambient temperature.

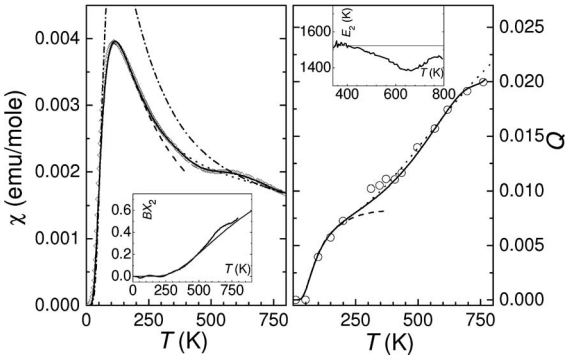

FIG. 5. Left panel: the corrected magnetic susceptibility of $LaCoO_3$. Right panel: the anomalous part of the thermal expansion of $LaCoO_3$ at ambient pressure. The dashed line represents the fit by the LS-IS model without orbital degeneracy ($\nu_1=3$), dotted line — the fit by the LS-IS-HS model without orbital degeneracy ($\nu_1=3$ and $\nu_2=5$) with fixed E_1, E_2, solid line—the fit by the LS-IS-HS model with a temperature-dependent E_2, dash-dotted line—the fit by the orbitally degenerate LS-IS-HS model ($\nu_1=9$ and $\nu_2=15$). The inset in the left panel: the temperature dependence of $Bx_2=(\chi T-AQ)$ (black line) and its fit using Eq. (3) (gray line). Inset in the right panel: the temperature dependence of the LS-HS energy splitting E_2.

about an order of magnitude only. For the energy-splitting value between the ground state and first excited state of about 180 K,[16–18] the non-negligible population of the second excited state is expected for the $T>300$ K range and it should be properly taken into account for the description of physical properties of $LaCoO_3$ at the high-temperature range.

In the three-level model[13,7] the χ and Q can be written as

$$\chi = \frac{N_A g^2 \mu_B^2}{3k_B T}[S_1(S_1+1)x_1 + S_2(S_2+1)x_2], \tag{2}$$

$$Q = Q_1 x_1 + Q_2 x_2. \tag{3}$$

Here N_A is the Avogadro number, μ_B is the Bohr magneton, k_B is the Boltzmann constant, $S_1=1$, $S_2=2$ are the spin values and x_1, x_2 are the populations corresponding to IS and HS states of the Co^{3+} ions. We have chosen the g-factor value of 2.1 obtained from a previous susceptibility analysis in the two-level LS-IS model.[16] The coefficients Q_1 and Q_2 are related to the change of the equilibrium unit-cell volume due to the change of the spin state, IS, and HS. The populations of the IS and HS states are determined by the degeneracy factors and LS-IS and LS-HS energy splittings as

$$x_{1,2} = \nu_{1,2}\exp(-E_{1,2}/k_B T)/[1+\nu_1\exp(-E_1/k_B T) + \nu_2\exp(-E_2/k_B T)]. \tag{4}$$

The degeneracy factors $\nu_1=3$ for the IS and $\nu_2=5$ for the HS states were chosen assuming that their orbital degeneracy is lifted by local structural distortions.[16–18] The level splitting due to the trigonal crystal field of ~6 K (Ref. 21) is much smaller than the LS-IS energy separation ~180 K (and also the expected LS-HS one) and it can be neglected for simplicity.

The temperature behavior of the magnetic susceptibility and anomalous thermal expansion in the low-temperature range is mainly determined by the growing population x_1 of the IS state with a considerably smaller energy splitting than that expected for the HS one. Neglecting the population of the HS state x_2 at low temperatures, one can get the LS-IS energy splitting E_1 from the fit of the susceptibility and thermal expansion data (Fig. 5) using expression $x_1=\nu_1\exp(-E_1/k_B T)/[1+\nu_1\exp(-E_1/k_B T)]$ and Eqs. (2) and (3). The obtained value $E_1=185$ K is in good agreement with one found in Refs. 16–18. With a given E_1 value, the susceptibility and thermal expansion are well described in the temperature range up to about 250 K and at higher temperatures the experimental and calculated curves start to deviate from each other with a growing difference, indicating that the population of the HS state starts to increase at $T>250$ K only. Using the obtained $x_1(T)$ dependence, one can get the $x_2(T)$ dependence from the system of linear equations (2) and (3) with unknown coefficients Q_1 and Q_2. If one chooses the constant $A=N_A g^2 \mu_B^2 S_1(S_1+1)/3k_B Q_1$ in such a way that quantity $(\chi T-AQ)$ is equal to zero and temperature independent in the low-temperature range, at $T>250$ K this quantity will be proportional to x_2, as it comes from Eqs. (2) and (3). The obtained temperature dependence of $(\chi T-AQ)=Bx_2$ $[B=N_A g^2 \mu_B^2 S_2(S_2+1)/3k_B-AQ_2]$ is shown in Fig. 5 (inset). It can be well described with $Q_1=0.013$, $Q_2=0.07$, $E_1=185$ K, and $E_2=1520$ K at temperatures below 450 K. The relative difference between E_2 and E_1 values of about eight times is comparable with the LDA+U calculation predictions.[12]

At higher temperatures the calculated curve with a fixed E_2 value shows a slight nonlinear deviation from the experimental Bx_2 dependence. This indicates a presence of two processes in the behavior of the population of the HS state x_2 with a temperature increase—a broad-range thermal excitation and a sharper change due to the semiconductor-metal transition at $T>450$ K. For the better description of the experimental data, one can assume that the E_2 value undergoes some change in the vicinity of the S-M transition. The $E_2(T)$ dependence calculated with Eq. (3) and $Bx_2(T)$ dependence is shown in Fig. 5 (inset). It decreases from the initial 1520 K value to about 1380 K in the temperature range 450–650 K and increases at higher temperatures back to about 1500 K. The populations of the IS and HS states finally calculated from Eqs. (2) and (3) for the models with the fixed E_1, E_2 values and also with $E_2(T)$ dependence (Fig. 5) are shown in Fig. 6. They differ rather little in the S-M transition region.

In addition we also tested the model with orbitally degenerate IS and HS states with $\nu_1=9$ and $\nu_2=15$. It gives a significantly worse fit of the susceptibility in comparison with the LS-IS-HS model without orbital degeneracy (see Fig. 5).

The quantity $Q=(V-V_T)/V_T$, characterizing the anomalous thermal expansion of the unit-cell volume due to spin-state transitions contains the normal thermal expansion term V_T due to phonons. The V_T value depends on the unit-cell volume at $T=0$, thermal expansion coefficient, and Debye temperature.[7] Among these, the high pressure affects most

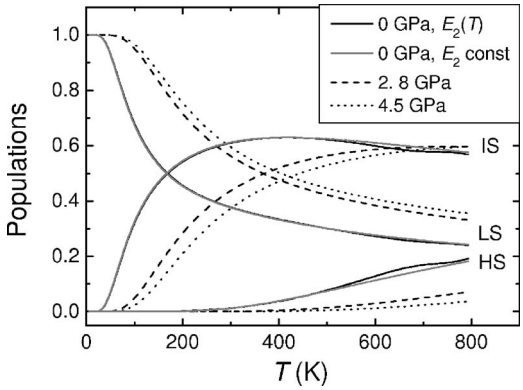

FIG. 6. The populations of LS, IS, and HS states at ambient and high pressures.

strongly the unit-cell volume, while two latter parameters are rather weak functions of pressure.[46,47] Therefore in a good approximation the V_T value for the considered pressure range up to 4.5 GPa can be calculated by simple scaling of the unit-cell volume at $T=0$ obtained from low-temperature data. The obtained in such a way $Q(T)$ dependences at different pressures for low-temperature (16–250 K) and high-temperature (300–905 K) ranges are shown in Fig. 7.

Since the population of the HS state in the 16–250 K temperature range is close to zero, low-temperature $Q(T)$ data were used for the calculation of E_1 and Q_1 parameters (Table I) with Eqs. (2) and (3). Subsequently, the E_2 and Q_2 parameters (Table I) were refined from high-temperature data using the known pressure behavior of E_1 and Q_1 values. The good description of the experimental data with the temperature-independent E_1, E_2 values was obtained (Fig. 7). Both LS-IS and LS-HS energy splittings increase substantially under high pressure (Fig. 8) with a larger $d\ln E_1/dP=0.37$ GPa^{-1} value in comparison with $d\ln E_2/dP=0.23$ GPa^{-1}. The obtained value of $d\ln E_1/dP$ is comparable with the averaged $d(\ln \Delta_1)/dP \approx 0.5$ GPa^{-1} evaluated for the volume-independent part of the LS-IS energy splitting from the magnetization measurements for the

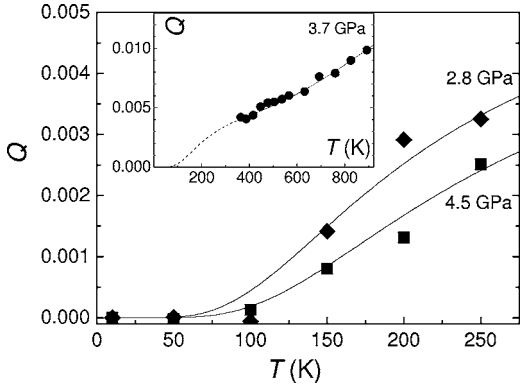

FIG. 7. The anomalous part Q of the thermal expansion of $LaCoO_3$ at different pressures obtained in the low-temperature 10–250 K and high-temperature 300–900 K (inset) ranges. The solid lines represent the LS-IS-HS model fits as described in the text. The dashed line in the inset is the expected low-temperature behavior of Q at $P=3.7$ GPa.

TABLE I. The obtained LS-IS, LS-HS splitting energies and Q_1, Q_2 parameters at different pressures for $LaCoO_3$.

P (GPa)	E_1 (K)	E_2 (K)	Q_1	Q_2
0	185	1520	0.0130	0.070
2.8	405		0.0088	
3.7	445[a]	2820	0.0085[a]	0.069
4.5	485		0.0083	

[a]Calculated from experimental $E_1(P)$ and $Q_1(P)$ dependences.

smaller pressure range 0–1.8 GPa in the LS-IS model with elastic energy contribution.[30] In that approach some deviation of the $\Delta_1(P)$ dependence from the linear law characteristic for our $E_1(P)$ data was found.

The calculated temperature dependences of the LS, IS, and HS states populations under high pressure are shown in Fig. 6. They were obtained assuming the linear pressure dependence of E_1 and E_2 parameters (Table I). With increasing pressure the IS and HS states are depopulated in favor of the LS ground state. In the low-temperature region $T<250$ K, where the population of the HS state is negligible, the population of the LS state progressively increases and that for the IS state decreases.

For ambient pressure it was found that the spin-state transitions affect mostly the thermal expansion of the Co-O bond length while the Co-O-Co bond angle temperature dependence follows the normal way expected from the phonon contribution only.[7] We also found that the temperature dependences of the Co-O bond length at different pressures resemble the unit-cell volume expansion containing the additional contribution due to spin-state transitions while those of the Co-O-Co bond angle do not exhibit any anomalies.

B. Raman spectra and semiconductor-metal transition

The Raman spectra of $LaCoO_3$ measured at selected temperatures under the external sample heating are shown in

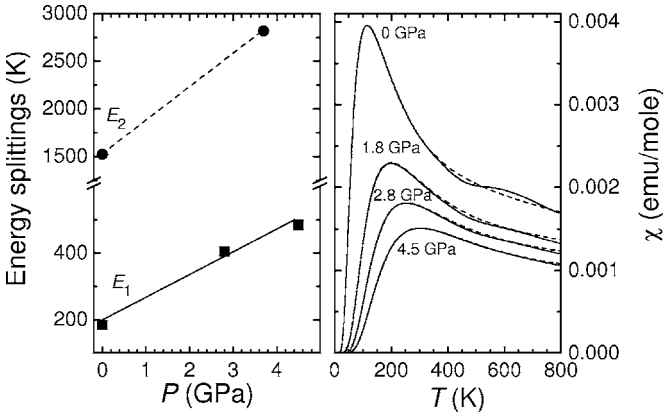

FIG. 8. Left panel: pressure dependences of the LS-IS and LS-HS energy splittings. Right panel: the calculated temperature curves of magnetic susceptibility at different pressures with constant LS-IS and LS-HS (dashed curves) and temperature-dependent LS-HS (solid curves) energy splittings.

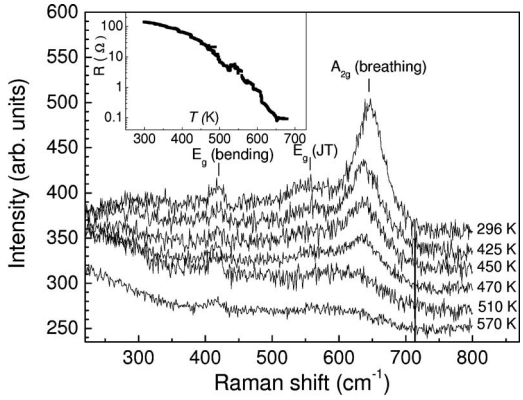

FIG. 9. Temperature dependencies of Raman spectra and resistivity (inset) of $LaCoO_3$ at ambient pressure.

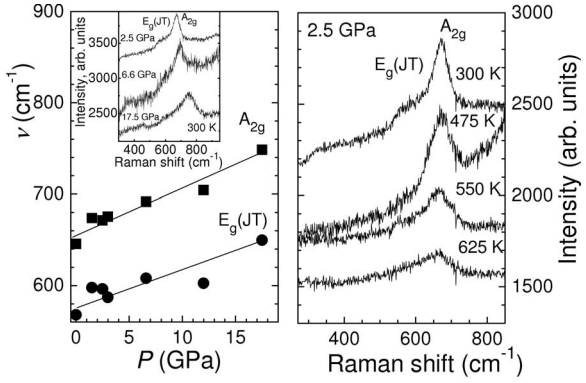

FIG. 10. Left panel: pressure dependences of A_{2g} breathing and quadrupole (JT) E_g mode frequencies of $LaCoO_3$ and Raman spectra of $LaCoO_3$ at different pressures and ambient temperature (inset). Right panel: temperature dependencies of Raman spectra of $LaCoO_3$ at $P=2.5$ GPa.

Fig. 9. Two broad modes and a sharper mode, located at ~645, 565, and 420 cm^{-1}, respectively, were observed. In the notation of work,[27] they can be assigned to A_{2g} breathing, E_g quadrupole (JT) and E_g bending modes. In the rhombohedrally distorted perovskite structure of the $R\bar{3}c$ symmetry the Raman active modes are $A_{1g}+4E_g$. The observation of the A_{2g} and quadrupole (JT) E_g modes inactive for the $R\bar{3}c$ indicates the presence of the distortions lowering the symmetry of the local crystal structure. The JT distortions and relevant e_g orbital order of Co^{3+} ions in the IS state may be an origin of the local symmetry lowering.[12,20,27]

A sharp decrease of the A_{2g} breathing and quadrupole (JT) E_g modes intensities was observed at $T>425$ K. It correlates with the drop of the dc resistivity during the S-M transition (Fig. 9, inset), which was measured simultaneously with the Raman spectra. At $T>570$ K both peaks nearly disappear. A similar effect was also observed in the experiments with a laser surface heating,[29] although in that study the resistivity behavior with the temperature increase was not controlled and the sample surface temperature was estimated from the anti-Stokes Raman signal only.

The Raman spectra of $LaCoO_3$ in the metallic phase resemble that of metallic rhombohedral $La_{1-x}Sr_xCoO_3$ (Ref. 27) with one resolved E_g bending mode in the 250–900 cm^{-1} range and become consistent with the $R\bar{3}c$ symmetry. The suppression of the local distortions characteristic for the semiconducting phase would be a reason for the observed change of the LS-HS energy splitting during the gradual S-M transition.

The Raman spectra of $LaCoO_3$ at ambient temperature and high pressures up to 17.5 GPa (Fig. 10, inset) are similar to those obtained at ambient pressure. Due to additional background from diamond anvils, the peak with a smallest intensity corresponding to the E_g bending mode located at ~420 cm^{-1} cannot be resolved with a desirable accuracy. The frequencies of the A_{2g} breathing and quadrupole (JT) E_g modes increase nearly linearly under pressure (Fig. 10). The calculated Grüneisen parameter $\gamma_i=-\partial(\ln \nu_i)/\partial \ln V$ values for these modes are 1.3 and 1.0, respectively. The values $\gamma \geq 1$ are characteristic for internal vibrational modes, while the case $\gamma<1$ generally corresponds to external modes, such as rigid rotations.[48]

At $P=2.5$ GPa on heating a sharp decrease of the A_{2g} breathing and quadrupole E_g (JT) modes intensities was observed at $T\sim550$ K (Fig. 10). Since a suppression of these modes correlates with the gradual S-M transition, this implies the noticeable increase of the S-M transition temperature from 425 to 550 K with $dT_{S\text{-}M}/dP\approx50$ K/GPa.

IV. DISCUSSION

Previously, spin-state transitions in $LaCoO_3$ were analyzed in terms of the three-level LS-IS-HS model with elastic energy contribution[13,7] and also the two-level LS-IS model.[16–18] The LS-IS-HS model with volume-dependent elastic energy terms incorporated to LS-IS and LS-HS splittings could not correctly reproduce the temperature behavior of the magnetic susceptibility and thermal expansion. Only the introduction of additional correction terms in rather arbitrary form dependent on the population of the HS state x_2 (Ref. 13) or on both IS and HS states x_1 and x_2 (Ref. 7) improves the description of the experimental data. However, such a correction affects strongly the temperature dependence of energy splittings, so the LS-HS splitting changes nearly by an order of magnitude in the 0–800 K range,[13] while without such corrections both splittings were much weaker functions of temperature. The two-level LS-IS model with a constant energy splitting was found to work well for intermediate temperatures $T<350$ K, but it fails to reproduce consistently the behavior of the susceptibility and thermal expansion at higher temperatures. To overcome this, either a change of the degeneracy of the IS state from 3 to 9 or an unreasonably strong T dependence of the LS-IS energy splitting changing from 200 to 2000 K in the 0–1000 K temperature range were assumed.[16,17] However, the LS-IS model remains to be inconsistent with the particular behavior of x-ray absorption and photoemission spectra[8–10,14,15] as well as the considerable increase of the effective paramagnetic moment in the vicinity of the high-temperature susceptibility anomaly.[4]

In the present study by solving of the system of linear equations (2) and (3) without *a priori* model assumptions

about volume or temperature dependence of energy splittings, we found that the susceptibility and thermal expansion of $LaCoO_3$ can be successfully described with the constant LS-IS and weekly temperature-dependent LS-HS energy splittings. This implies that the contribution of the elastic energy to energy splittings considered in[13,7] and neglecting the possibility of local site relaxation, is an overestimation.

An alternative scenario of the spin-state transitions in $LaCoO_3$ was recently proposed from ESR data.[21] The observed at low $T<50$ K first excited triplet state of Co^{3+} with the zero-field splitting of 0.6 meV was attributed to the HS state, which splits by spin-orbit coupling into the lowest-lying triplet and higher-lying quintet and septet corresponding to the effective total angular momentum values $\tilde{J}=1$, 2, and 3.[21,22] The splittings between triplet and quintet and quintet and septet are 2λ and 3λ, where the spin-orbit coupling constant $\lambda \approx 150$ cm$^{-1}=215$ K.[22] With a triplet located at $E\sim 180$ K above the ground state one can get the susceptibility values several times exceeding the experimental ones with g factors values of 3.5 or even 2. The IS state is expected to split by spin-orbit coupling into singlet, triplet, and quintet with a lowest quintet.[22] The distance between quintet and triplet is similar to that of the HS case and the singlet state is nonmagnetic. The calculated susceptibility for this case also gives several times overestimation in comparison with the experimental data.

In this and previous investigations[7,13,16–18] it was found that the susceptibility of the $LaCoO_3$ in the extended temperature range can be described reasonably well with the g-factor value $g\sim 2$. The $g=2$ was also found from the ESR study of the related compound $La_{0.9}Sr_{0.1}CoO_3$.[49] The $La_{0.9}Sr_{0.1}CoO_3$ is paramagnetic over the 0–800 K temperature range with Co^{3+} ions in the IS state and it does not exhibit spin-state transitions.[50] The contrasting ESR value[21] $g\sim 3.5$ obtained at low temperatures implies a possible dependence of the electronic configuration of Co^{3+} ions in $LaCoO_3$ on the population of the magnetic excited states. For the temperature range $T<50$ K of the ESR study[21] a number of Co^{3+} ions in the first magnetic excited state $x_1<7\%$, and they are expected to behave like isolated noninteracting impurity centers imbedded in the nonmagnetic LS ions lattice with negligible electron-electron correlation effects due to p-d hybridization with oxygen ligands. For this case, a thermal excitation of the localized electronic levels stabilized by spin-orbit coupling is quite natural. The relevant electronic configuration of Co^{3+} may be described as the spin-orbit split HS state with a considerable contribution to the g-factor value from orbital momentum.

With a further temperature increase the population of magnetic Co^{3+} ions grows rapidly and the formation of lattice states (bands) occurs. Due to enhanced hybridization between Co e_g and O $2p$ orbitals the IS state is stabilized, as found from LDA+U calculations[12] and supported by numerous recent investigations.[13–20] The HS state has less hybridization channels and it is shifted to higher energies in comparison with the IS one.[12] Such a scenario is supported by Raman spectroscopy[27] and inelastic neutron-scattering investigations,[51] which have shown that phonon modes associated with CoO_6 octahedra vibrations remain nearly constant for $T<50$ K but they undergo remarkable softening at higher T over the whole Brillouin zone. These observations reflect the appearance of local intramolecular distortions expected for the JT effects associated with the populated IS state. These distortions along with the strong p-d hybridization between O and Co ions are expected to reduce the orbital momentum contribution to the total angular momentum and lift orbital degeneracy.[22,12,16–18] The lifting of orbital degeneracy is also expected for the HS state since its population occurs in the distorted structural network of surrounding Co^{3+} ions in the IS state. Thus, for intermediate and high-temperature range ($T>50$ K) the approach with threefold and fivefold spin degenerate and orbitally nondegenerate magnetic excited states of IS and HS nature and $g\sim 2$ seems to be more appropriate for the description of magnetic susceptibility and thermal expansion of $LaCoO_3$. It is also in better agreement with photoemission and x-ray absorption spectroscopy results, implying a different electronic configuration of Co^{3+} ions in two magnetic excited states.[8–10,14,15]

From a conventional ligand field theory, using the crystal-field splitting value of about 2 eV (Ref. 15) at ambient pressure and the pressure dependence of the Co-O distance one can estimate with Tanabe-Sugano diagrams[22] the changes in E_1, E_2 due to the increase of the crystal-field splitting to be about $d\ln E_{1,2}/dP\sim 0.95$ and 0.28 GPa^{-1}, respectively, for the ideal cubic octahedral geometry. While this theory gives a reasonable estimation comparable with the experimental value $d\ln E_2/dP=0.23$ GPa^{-1} for the HS state, its prediction for the IS state is more than twice larger than the experimental value $d\ln E_1/dP=0.37$ GPa^{-1}. It is well known that from the conventional ligand field theory only LS and HS ground states are possible.[22] The IS state is stabilized by strong hybridization between $3d$ orbitals of cobalt and $2p$ orbitals of oxygen[12] and consideration of this effect would give a more reasonable estimation for the high-pressure behavior of LS-IS energy splitting.

The observation of the A_{2g} and quadrupole (JT) E_g modes forbidden for the $R\bar{3}c$ symmetry in the Raman spectra of $LaCoO_3$ over the 0–17.5 GPa pressure range and ambient temperature reflects the presence of the local structural distortions associated with the e_g orbital order of Co^{3+} ions in the IS state.[12,20,27] While from the high-resolution x-ray-diffraction data[23] the long-range character of the e_g orbital order was claimed but later inelastic neutron-scattering investigations[20] were consistent with the short-range character of the orbital order. Additional insight in the e_g orbital order nature can be obtained from the neutron diffraction data, which provides a much more sensitive probe of the oxygen structural parameters in the presence of heavy atoms than the x-ray diffraction. For this purpose, we treated the diffraction pattern obtained at ambient conditions (Fig. 2) using the alternative monoclinic structural model of the $I2/a$ symmetry, proposed from the x-ray-diffraction study.[23] In this model there are three pairs of nonequivalent Co-O bonds, the out-of-plane Co-O1 and in the ab plane the Co-O2$_{a,b}$. For a comparison, in the conventional rhombohedral model CoO_6 octahedra are isotropic with equivalent values of all bond lengths Co-O and angles Co-O-Co. Both models give nearly the same refinements quality with R_p

$=8.48\%$, $R_{wp}=7.43\%$ ($R\bar{3}c$), and $R_p=8.51\%$, $R_{wp}=7.4\%$ ($I2/a$). Although the unit-cell parameters obtained for the monoclinic model, $a=5.3835(8)$ Å, $b=5.4252(8)$ Å, $c=7.6824(14)$ Å, and $\beta=91.09(3)°$ are similar to those from Ref. 23, the relative difference between the Co-O bond lengths, $l_{\text{Co-O1}}=1.930(3)$ Å, $l_{\text{Co-O2a}}=1.924(3)$ Å, and $l_{\text{Co-O2b}}=1.937(3)$ Å is much smaller than that found in Ref. 23. The average values of the Co-O distances and Co-O-Co angles, $l_{\text{Co-O}}=1.930$ Å and $\varphi_{\text{Co-O-Co}}=165.33°$, as well as the unit-cell volume per molecular unit $V_m=56.084$ Å^3, are nearly identical to that of the rhombohedral model, $l_{\text{Co-O}}=1.930$ Å, $\varphi_{\text{Co-O-Co}}=165.30°$, and $V_m=56.085$ Å^3. The calculated distortion parameter $\delta_{\text{JT}}=\sqrt{\frac{1}{3}\Sigma_i[(l_{\text{Co-O}})_i-\langle l_{\text{Co-O}}\rangle]^2}=0.0053$ Å is comparable with one[52] 0.0026 Å for the orthorhombic $CaMnO_3$, which contains JT inactive Mn^{4+} ions and much smaller than that found from the x-ray diffraction for $LaCoO_3$ at ambient temperature, $\delta_{\text{JT}}=0.0488$ Å.[23] For a comparison, in the case of the classical JT system $LaMnO_3$ with the static long-range e_g orbital order the value $\delta_{\text{JT}}=0.1139$ Å was obtained from neutron diffraction data of similar quality.[53] Therefore, the small value of δ_{JT} obtained from our data supports the conclusion of the inelastic neutron-scattering study[20] that the e_g orbital order in $LaCoO_3$ due to JT distortions has the short-range dynamic character, in contrast to the x-ray-diffraction result.[23]

The obtained from structural data pressure dependencies of LS-IS and LS-HS energy splittings $E_{1,2}$ (Table I) and $E_2(T)$ dependence (Fig. 5) allow one to calculate the magnetic susceptibility of $LaCoO_3$ at different pressures (Fig. 8). A large decrease of the maximum of the low-temperature susceptibility peak, its broadening and shift to higher temperature are found. For the temperature range up to 350 K, these features are in good agreement with the behavior of the experimental susceptibility data[30] obtained at high pressures up to 1.8 GPa. The high-temperature anomaly in calculated curves becomes less pronounced and for $P>1.8$ GPa the results obtained with temperature-dependent and constant E_2 are nearly identical. Such a behavior correlates also with the absence of the well-defined high-temperature anomaly in the experimental anomalous thermal expansion data obtained at $P=3.7$ GPa (Fig. 7) and it can be explained by a substantial increase of both $E_{1,2}$ energy splittings under pressure.

It is interesting to compare pressure-induced changes of the LS-IS energy splittings and the S-M transition temperature in $LaCoO_3$ with chemical substitution effects in $La_{1-x}Eu_xCoO_3$ compounds (isostructural for $x<0.25$),[17] also leading to the decrease of the unit-cell volume. As in Ref. 17 only the LS-IS energy splitting as a function of Eu doping was analyzed, no comparison can be made for the LS-HS one. The values $d\ln E_1/d\ln V=-97$ and $d\ln T_{\text{S-M}}/d\ln V=-4.5$ for $La_{1-x}Eu_xCoO_3$ are drastically different from those corresponding to the application of high pressure for $LaCoO_3$, $d\ln E_1/d\ln V=-56$ and $d\ln T_{\text{S-M}}/d\ln V=-18$. It is known that the reduction of the R-cation ionic radius in $RCoO_3$ leads to the pronounced decrease of the Co-O-Co bond angle, while the Co-O bond length remains nearly unchanged.[54] In contrast, the application of high external pressure leads mostly to the decrease of the Co-O bond length, while the Co-O-Co angle increases rather weakly. Such contrasting structural responses due to chemical substitution and the application of high pressure result in the different modification of the p-d hybridization strength and charge carriers bandwidth and consequently in different behavior of LS-IS energy splitting and $T_{\text{S-M}}$ values as functions of the unit-cell volume.

The resistivity (Fig. 9) and thermopower[55] of $LaCoO_3$ do not show a sharp but rather a smooth decrease during the gradual semiconductor-metal transition. Such a behavior implies that the S-M transition goes through a formation of a phase-separated mixture where the volume fraction of metallic clusters grows gradually to beyond percolation with a temperature increase.[55] The metallic clusters are assumed to occur due to the transformation of localized σ bonding e_g states of IS Co^{3+} ions into the itinerant electron σ^* band.[55] Such a mechanism is supported by the disappearance of vibrational modes forbidden for the $R\bar{3}c$ symmetry and associated with the JT active IS Co^{3+} ions at the S-M transition. The considerable increase of the LS-IS energy splitting under high pressure leads to the sharp depopulation of the IS state and the rapid increase of the S-M transition temperature. Generally the thermally driven S-M transition is characterized by negative $dT_{\text{S-M}}/dP$ values in transition-metal oxides.[56] In contrast, a positive $dT_{\text{S-M}}/dP\approx 50$ K/GPa value was obtained for $LaCoO_3$. This fact requires further detailed investigations.

V. CONCLUSIONS

The results of our study show that the susceptibility and thermal expansion of $LaCoO_3$ at high pressures can be described successfully by a thermal excitation of the LS cobalt species to orbitally nondegenerate magnetic states with different electronic configuration (IS and HS), while the model considering the excitation between spin-orbit multiplets belonging to the same magnetic state (either IS or HS) cannot reproduce the experimental data.

An application of high pressure leads mainly to the decrease of the Co-O bond lengths, while Co-O-Co bond angles change insignificantly. Such structural modifications lead to the rapid increase of energy splittings between the ground state and both excited states. The pressure behavior of LS-HS energy splitting is comparable with a prediction of a conventional theory for the crystal field with an ideal cubic octahedral geometry, while for the LS-IS one this theory gives about a twice large overestimation. This suggests the importance of the consideration of p-d hybridization effects for the latter case.

The semiconductor-metal transition correlates with the suppression of A_{2g} breathing and quadrupole (JT) E_g Raman modes forbidden for the ideal $R\bar{3}c$ symmetry and arising due to local structural distortions associated with the short-range e_g orbital order of Co^{3+} ions in the IS state. The Raman spectra of $LaCoO_3$ in the metallic phase resemble that of metallic doped $La_{1-x}Sr_xCoO_3$ compounds, indicating freezing out of the local structural distortions. The semiconductor-metal transition temperature increases substantially under high pressure, as a consequence of the depopulation of the IS state.

ACKNOWLEDGMENTS

The authors thank S. E. Kichanov, W. G. Marshall, and D. J. Francis for their help with experiments at DN-12 and Pearl/HiPr diffractometers and A. Yu. Kuznetsov and A. V. Kurnosov for their help with x-ray diffraction and Raman spectroscopy experiments. The allocation of the beam time and financial support from the ISIS facility and Bayerisches Geoinstitut are gratefully acknowledged.

[1] R. R. Heikes, R. C. Miller, and R. Mazelsky, Physica (Amsterdam) **30**, 1600 (1964).
[2] G. H. Jonker, J. Appl. Phys. **37**, 1424 (1966).
[3] P. M. Raccah and J. B. Goodenough, Phys. Rev. **155**, 932 (1967).
[4] M. A. Señarís-Rodríguez and J. B. Goodenough, J. Solid State Chem. **116**, 224 (1995).
[5] J. B. Goodenough, Prog. Solid State Chem. **5**, 145 (1971).
[6] G. Thornton, B. C. Tofield, and A. W. Hewat, J. Solid State Chem. **61**, 301 (1986).
[7] P. G. Radaelli and S.-W. Cheong, Phys. Rev. B **66**, 094408 (2002).
[8] S. Masuda, M. Aoki, Y. Harada, H. Hirohashi, Y. Watanabe, Y. Sakisaka, and H. Kato, Phys. Rev. Lett. **71**, 4214 (1993).
[9] M. Abbate, J. C. Fuggle, A. Fujimori, L. H. Tjeng, C. T. Chen, R. Potze, G. A. Sawatzky, H. Eisaki, and S. Uchida, Phys. Rev. B **47**, 16124 (1993).
[10] T. Saitoh, T. Mizokawa, A. Fujimori, M. Abbate, Y. Takeda, and M. Takano, Phys. Rev. B **55**, 4257 (1997).
[11] R. H. Potze, G. A. Sawatzky, and M. Abbate, Phys. Rev. B **51**, 11501 (1995).
[12] M. A. Korotin, S. Yu. Ezhov, I. V. Solovyev, V. I. Anisimov, D. I. Khomskii, and G. A. Sawatzky, Phys. Rev. B **54**, 5309 (1996).
[13] K. Asai, A. Yoneda, O. Yokokura, J. M. Tranquada, G. Shirane, and K. Kohn, J. Phys. Soc. Jpn. **67**, 290 (1998).
[14] G. Vankó, J.-P. Rueff, A. Mattila, Z. Németh, and A. Shukla, Phys. Rev. B **73**, 024424 (2006).
[15] M. Medarde, C. Dallera, M. Grioni, J. Voigt, A. Podlesnyak, E. Pomjakushina, K. Conder, Th. Neisius, O. Tjenberg, and S. N. Barilo, Phys. Rev. B **73**, 054424 (2006).
[16] C. Zobel, M. Kriener, D. Bruns, J. Baier, M. Grüninger, T. Lorenz, P. Reutler, and A. Revcolevschi, Phys. Rev. B **66**, 020402(R) (2002).
[17] J. Baier, S. Jodlauk, M. Kriener, A. Reichl, C. Zobel, H. Kierspel, A. Freimuth, and T. Lorenz, Phys. Rev. B **71**, 014443 (2005).
[18] K. Knížek, Z. Jirák, J. Hejtmánek, M. Veverka, M. Maryško, G. Maris, and T. T. M. Palstra, Eur. Phys. J. B **47**, 213 (2005).
[19] S. Stølen, F. Grønvold, H. Brinks, T. Atake, and H. Mori, Phys. Rev. B **55**, 14103 (1997).
[20] D. Phelan, D. Louca, S. Rosenkranz, S.-H. Lee, Y. Qiu, P. J. Chupas, R. Osborn, H. Zheng, J. F. Mitchell, J. R. D. Copley, J. L. Sarrao, and Y. Moritomo, Phys. Rev. Lett. **96**, 027201 (2006).
[21] S. Noguchi, S. Kawamata, K. Okuda, H. Nojiri, and M. Motokawa, Phys. Rev. B **66**, 094404 (2002).
[22] A. Abragam and B. Bleaney, *Electron Paramagnetic Resonance of Transition Ions* (Clarendon, Oxford, 1970), p. 21 and *Electron Paramagnetic Resonance of Transition Ions* (Clarendon, Oxford, 1970), p. 443.
[23] G. Maris, Y. Ren, V. Volotchaev, C. Zobel, T. Lorenz, and T. T. M. Palstra, Phys. Rev. B **67**, 224423 (2003).
[24] D. Louca and J. L. Sarrao, Phys. Rev. Lett. **91**, 155501 (2003).
[25] L. Sudheendra, M. M. Seikh, A. R. Raju, and C. Narayana, Chem. Phys. Lett. **340**, 275 (2001).
[26] S. Yamaguchi, Y. Okimoto, and Y. Tokura, Phys. Rev. B **55**, R8666 (1996).
[27] A. Ishikawa, J. Nohara, and S. Sugai, Phys. Rev. Lett. **93**, 136401 (2004).
[28] M. M. Seikh, L. Sudheendra, C. Narayana, and C. N. R. Rao, J. Mol. Struct. **706**, 121 (2004).
[29] N. Orlovskaya, D. Steinmetz, S. Yarmolenko, D. Pai, J. Sankar, and J. Goodenough, Phys. Rev. B **72**, 014122 (2005).
[30] K. Asai, O. Yokokura, M. Suzuki, T. Naka, T. Matsumoto, H. Takahashi, N. Mori, and K. Kohn, J. Phys. Soc. Jpn. **66**, 967 (1997).
[31] T. Vogt, J. A. Hriljac, N. C. Hyatt, and P. Woodward, Phys. Rev. B **67**, 140401(R) (2003).
[32] V. L. Aksenov, A. M. Balagurov, V. P. Glazkov, D. P. Kozlenko, I. V. Naumov, B. N. Savenko, D. V. Sheptyakov, V. A. Somenkov, A. P. Bulkin, V. A. Kudryashev, and V. A. Trounov, Physica B **265**, 258 (1999).
[33] V. P. Glazkov and I. N. Goncharenko, High Pressure Physics and Technics **1**, 56 (1991) (in Russian).
[34] Y. Le Godec, M. T. Dove, S. A. T. Redfern, M. G. Tucker, W. G. Marshall, G. Syfosse, and S. Klotz, High Press. Res. **23**, 281 (2003).
[35] D. Martinez-Garcia, Y. Le Godec, M. Mezouar, G. Syfosse, J. P. Itíe, and J. M. Besson, High Press. Res. **18**, 339 (2000).
[36] H. J. Stone, M. G. Tucker, Y. Le Godec, F. M. Méducin, E. R. Cope, S. A. Hayward, G. P. J. Ferlat, W. G. Marshall, S. Manolopoulos, S. A. T. Redfern, and M. T. Dove, Nucl. Instrum. Methods Phys. Res. A **547**, 601 (2005).
[37] V. B. Zlokazov and V. V. Chernyshev, J. Appl. Crystallogr. **25**, 447 (1992).
[38] R. B. Von Dreele and A. C. Larson, Los Alamos National Laboratory Report No. LAUR 86, 748, 1986 (unpublished).
[39] N. A. Dubrovinskaia and L. S. Dubrovinsky, Rev. Sci. Instrum. **74**, 3433 (2003).
[40] A. P. Hammersley, S. O. Svensson, M. Hanfland, A. N. Fitch, and D. Hausermann, High Press. Res. **14**, 235 (1996).
[41] J. Rodríguez-Carvajal, Physica B **192**, 55 (1993).
[42] F. J. Birch, J. Geophys. Res. **91**, 4949 (1986).
[43] R. Lengsdorf, M. Ait-Tahar, S. S. Saxena, M. Ellerby, D. I. Khomskii, H. Micklitz, T. Lorenz, and M. M. Abd-Elmeguid, Phys. Rev. B **69**, 140403(R) (2004).
[44] N. O. Golosova, D. P. Kozlenko, V. I. Voronin, and B. N. Savenko, Phys. Solid State **48**, 96 (2006).
[45] D. P. Kozlenko, I. N. Goncharenko, B. N. Savenko, and V. I. Voronin, J. Phys.: Condens. Matter **16**, 6755 (2004).
[46] L. S. Dubrovinsky, S. K. Saxena, F. Tutti, S. Rekhi, and T. Le Behan, Phys. Rev. Lett. **84**, 1720 (2000).
[47] L. S. Dubrovinsky, S. K. Saxena, N. A. Dubrovinskaia, S. Rekhi,

and T. Le Bihan, Am. Mineral. **85**, 386 (2000).
[48] A. Congeduti, P. Postorino, E. Caramagno, M. Nardone, A. Kumar, and D. D. Sarma, Phys. Rev. Lett. **86**, 1251 (2001).
[49] T. L. Phan, L. V. Bau, N. V. Khiem, N. X. Phuc, and S. C. Yu, Phys. Status Solidi B **242**, 1522 (2005).
[50] M. A. Señarís-Rodríguez and J. B. Goodenough, J. Solid State Chem. **118**, 323 (1995).
[51] Y. Kobayashi, T. S. Naing, M. Suzuki, M. Akimitsu, K. Asai, K. Yamada, J. Akimitsu, P. Manuel, J. M. Tranquada, and G. Shirane, Phys. Rev. B **72**, 174405 (2005).
[52] O. Chmaissem, B. Dabrowski, S. Kolesnik, J. Mais, D. E. Brown, R. Kruk, P. Prior, B. Pyles, and J. D. Jorgensen, Phys. Rev. B **64**, 134412 (2001).
[53] L. Pinsard-Gaudart, J. Rodríguez-Carvajal, A. Daoud-Aladine, I. Goncharenko, M. Medarde, R. I. Smith, and A. Revcolevschi, Phys. Rev. B **64**, 064426 (2001).
[54] J.-S. Zhou, J.-Q. Yan, and J. B. Goodenough, Phys. Rev. B **71**, 220103(R) (2005).
[55] J.-Q. Yan, J.-S. Zhou, and J. B. Goodenough, Phys. Rev. B **69**, 134409 (2004).
[56] M. Imada, A. Fujimori, and Y. Tokura, Rev. Mod. Phys. **70**, 1039 (1998).